Supplementary figures and tables

Table S1. Summary of timings of each inflection in the 3-step linear regression of annual bromine and MSA at Summit and Tunu. Regression was performed on the data sets with outliers removed as described in Fig. 2. The signs indicate the direction of the inflection in the record, errors are 2σ.

Timing of inflection (Year, C.E.)

	Infl. 1		Infl. 2		Infl. 3		Infl. 4
	Br	MSA	Br	MSA	Br	MSA	Br
Summit-2010	(-)1819 ±22	(-)1854 ±12	(+)1879 ±22	(+)1878 ±12	(+)1932 ±10	(-)1930 ±16	(-)1974 ±20
Tunu	(-)1842 ±22	(-)1812 ±12	(+)1857 ±24	(+)1821 ±21	(+)1944 ±18	(-)1984 ±4	(+)1966 ±20

Table S2. Summary of the average aerosol concentrations as determined by the 3-step linear regression of annual bromine and MSA at Summit and Tunu displayed in Fig. 2. The duration of each step in concentration is bracketed by the inflection points summarized in Table S1. Concentrations are in units of nM. MSA did not show a stable period after the third infection in the series and so was not assigned a concentration value for 'Step 3'. Errors represent 2σ in the concentration value.

Concentration (nM)

	Step 1		Step 2		Step 3
	Br	MSA	Br	MSA	Br
Summit-2010	5.4±0.2	48±1	4.2±0.2	36±2	5.5±0.3
Tunu	4.2±0.3	25±1	3.2±0.3	21.2±0.7	4.8±0.5

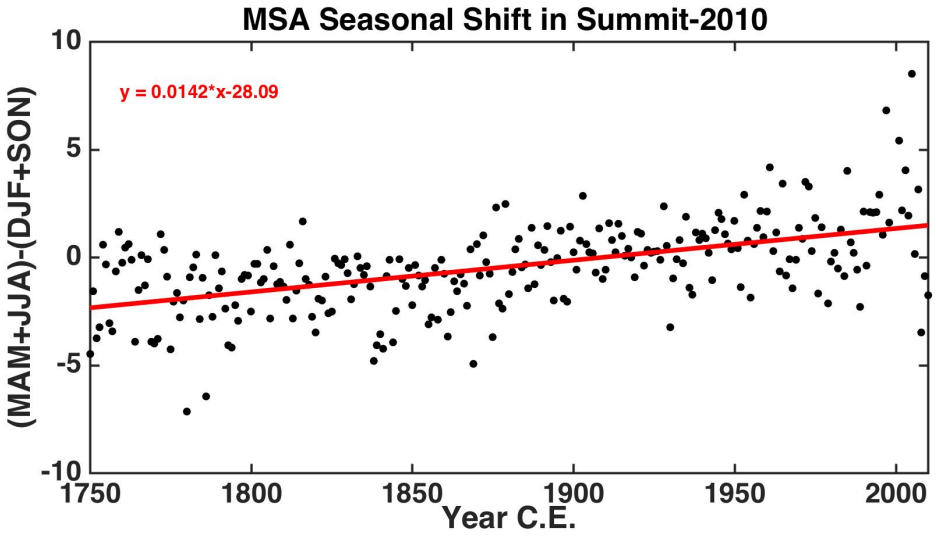

Figure S1. Illustration of the shift in the seasonal MSA peak along the length of the Summit-2010 ice core. The difference in amplitude between the spring/summer and winter/fall MSA signal each year was calculated ((MAM+JJA)-(DJF+SON)) and observed to shift linearly along the length of the ice core. At the shallowest, part of the ice core the positive values show the MSA peak appears in the spring/summer whilst in the deepest and oldest part of the ice core the signal has shifted to a winter/fall annual maximum. This phenomenon has previously been attributed to annual salt gradients within the ice core driving the migration of the MSA toward the higher salt location, winter (Mulvaney et al., 1992; Weller, 2004).

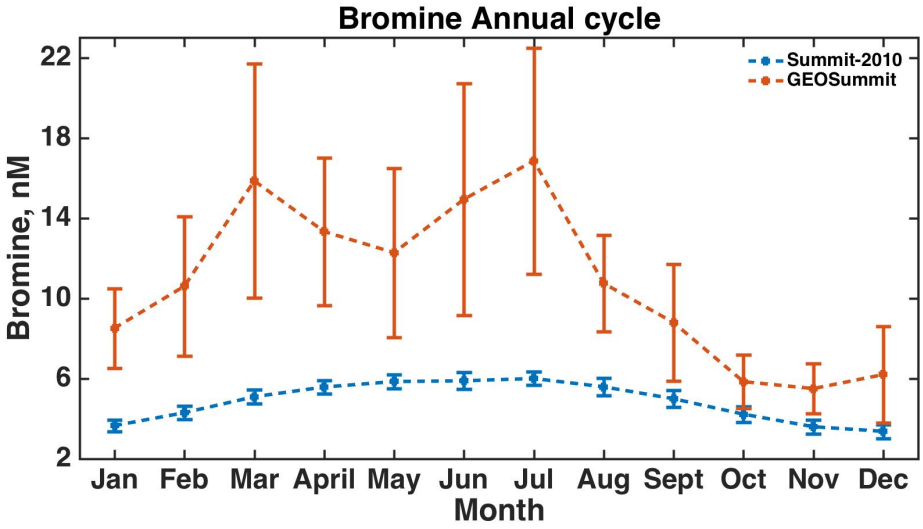

Figure S2. Comparison between the annual cycle in inorganic Br measured at Summit from snow samples taken as part of the GEOSummit project (2007-2013) and in the Summit-2010 ice core (1900-2010). The snow samples were analysed for inorganic Br on the same system used to measure the ice core records. The results of the snow samples support the observation from the ice cores that the maximum flux of Br is in summer with a possible secondary peak in spring. The error bars represent 1σ.

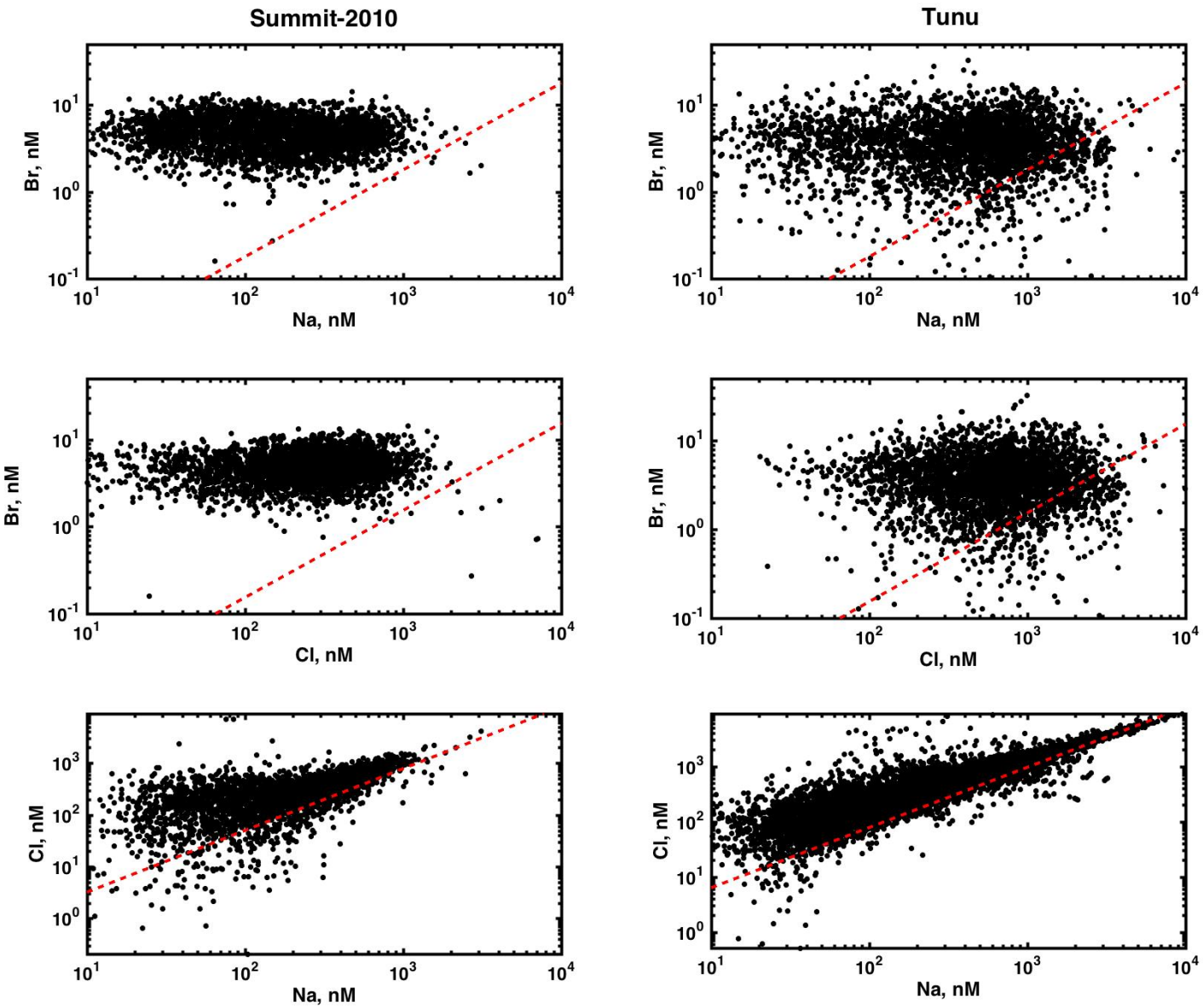

Figure S3. Monthly values of bromine, sodium and chlorine compared with their sea water ratio (red). At both sites, both the Br/Na and Br/Cl lie predominantly above the sea water ratio, whilst Cl/Na shows only a small Cl enrichment which increases at small sodium concentrations. At Tunu, 11% and 12% of the points show bromine depletion relative to Na and Cl, respectively. $([Br]/[Na])_{seawater}$ = 1.793x10^{-3}, $([Br]/[Cl])_{seawater}$ = 1.539x10^{-3}. $([Cl]/[Na])_{seawater}$ = 1.165

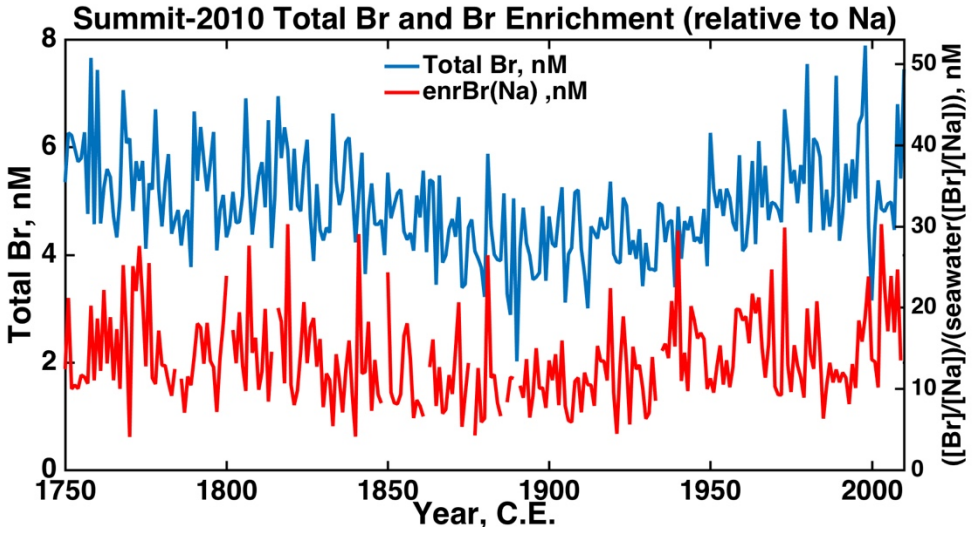

Figure S4. Total bromine and bromine enrichment (relative to sodium) from the Summit-2010 ice core.

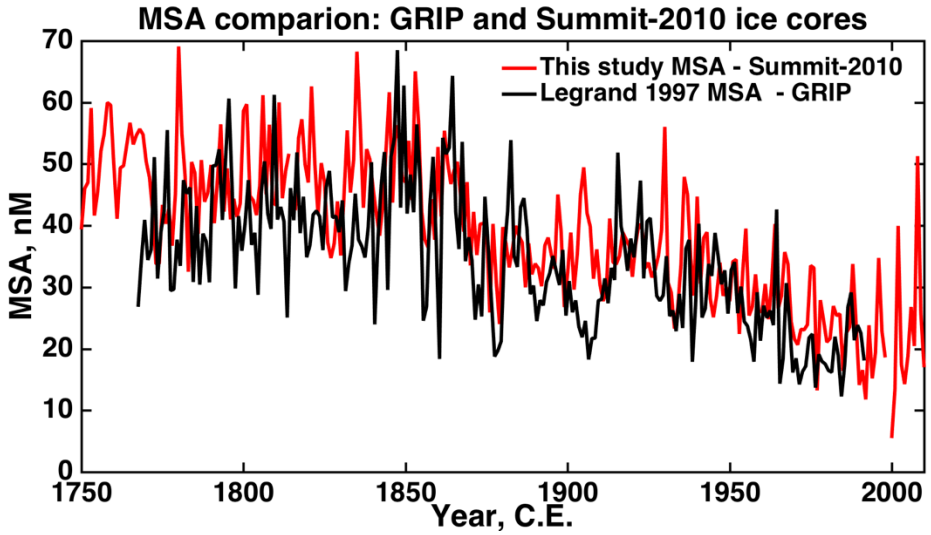

Figure S5. Comparison between the MSA record obtained from the GRIP ice core (Legrand et al., 1997) in 1993 and the Summit-2010 ice core from this study. The Summit-2010 ice core drill-site (72°20'N 38°17'24"W) is located 35 km SW of the GRIP ice core drill-site (72°34'N, 37°38'W). The GRIP MSA was measured in discrete samples using ion chromatography compared with the Summit-2010 ice core which was measured using the new technique of continuous melting of the ice core combined with continuous analysis by electrospray triple-quad mass spectrometry (as described in the text). The tight overlap between low frequency trend of the two series demonstrates that the new, continuous measurement technique is able to achieve a comparable accuracy in MSA concentration measurements to the discrete technique. It also demonstrates that negligible amounts of MSA are being lost during the continuous melt method. Discrepancies between the high frequency features of the two records is expected as the measurement resolution of the continuous method is much higher than the discrete method and the two records are from different ice core sites.

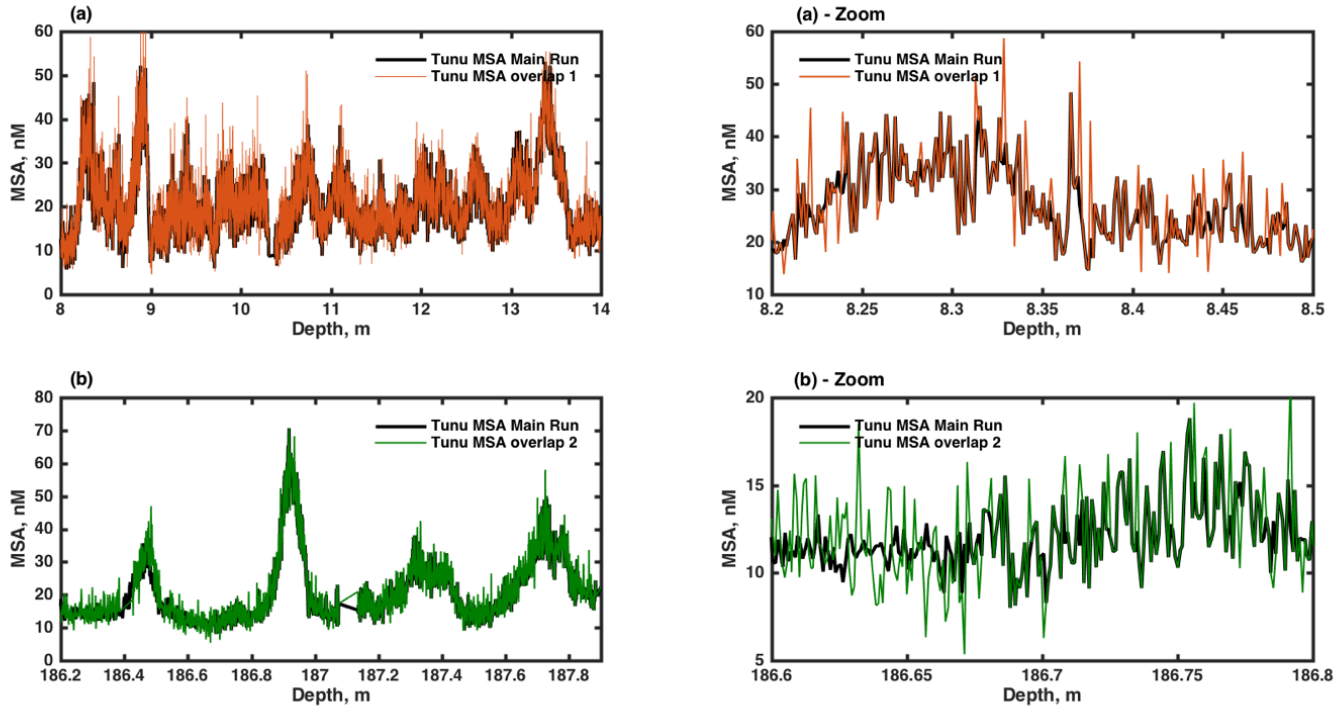

Figure S6. Demonstration of the reproducibility of the MSA online, continuous measurements performed on the Tunu ice core. Two different depths of the Tunu ice core are shown where the replicate analysis was performed by melting a secondary stick of ice cut from the same ice core and overlapping in depth ('overlap' ice sticks) : (a) Six 'overlap' ice sticks were melted sequentially to replicate the MSA record over the depth 8-14 m.(b) Two 'overlap' ice sticks were melted sequentially over the depth 186.2-187.9 m. Zooming in on a small section of the record at each depth demonstrates that the high frequency signal is real (not noise) and well replicated by the continuous MSA technique.

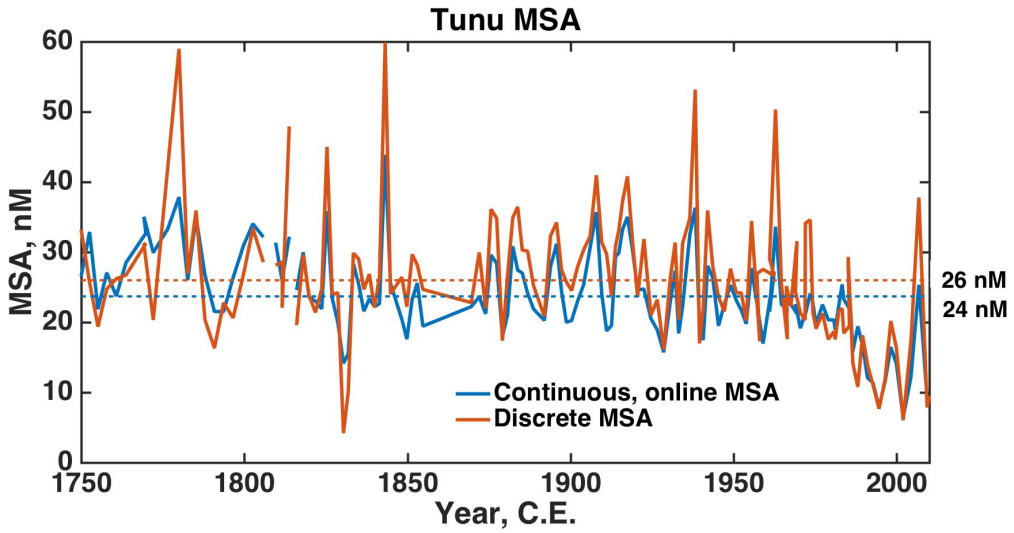

Figure S7. Comparison between discrete and continuous, online measurements of MSA measurements from the Tunu ice core samples. The discrete samples were collected as the continuous measurements were performed by directing part of the sample stream into an auto-sampler collection system just before they entered the analyzer. The samples were then frozen and later measured using ion chromatographic separation and the ESI-MS-MS detection. In this plot the continuous data have been averaged over the same depth range covered by each discrete sample and then both series plotted as the average age over that depth range. Over the 1750-2012 period the Tunu discrete measurements were, on average, 7% higher than the online measurements (dashed lines indicate average values over the 1750-2012 period). Both the discrete and continuous samples experienced identical conditions from ice melt to collection so the reason for offset in measured concentration is likely due to differences in post-processing of the data.

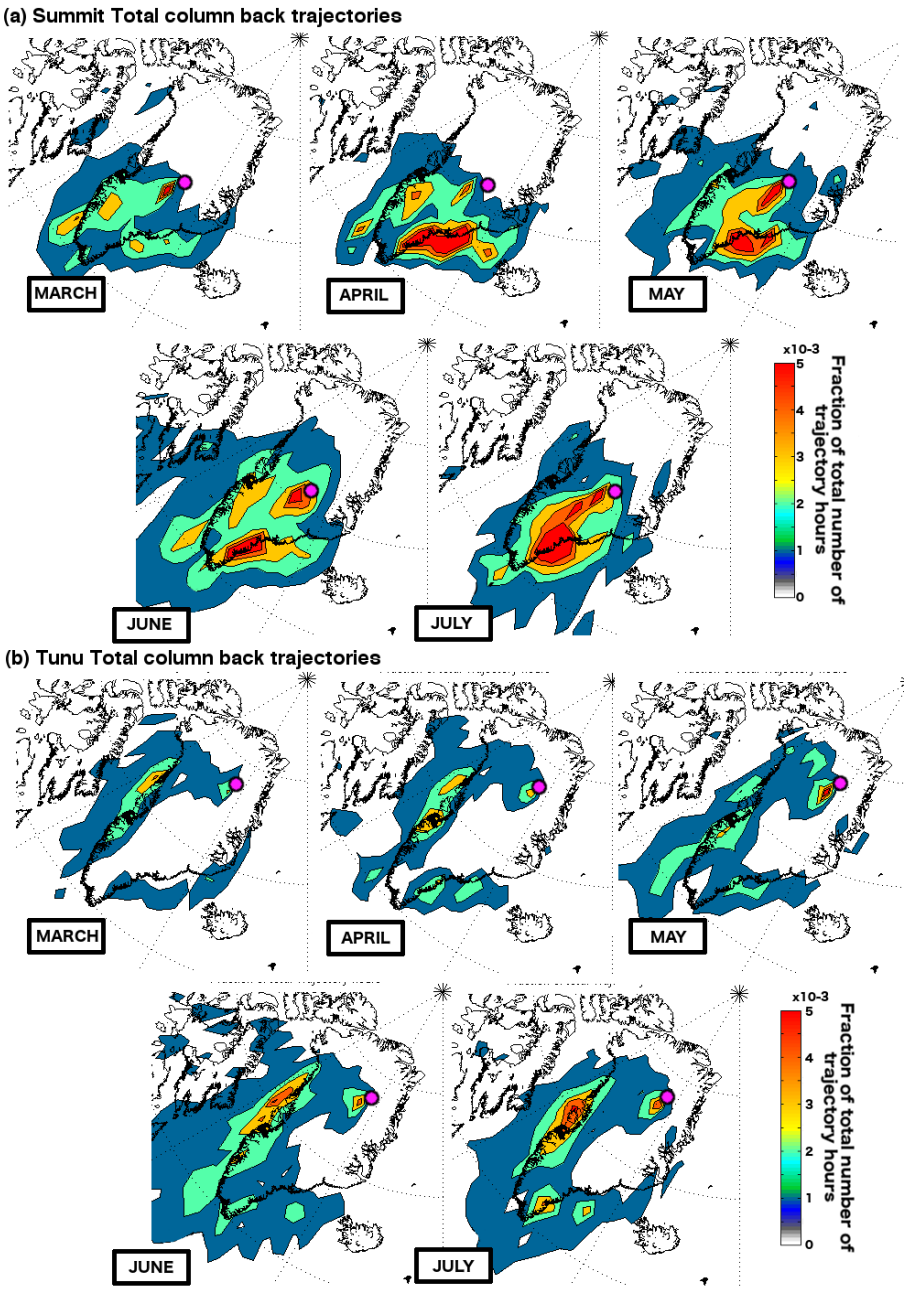

Figure S8. Total column air mass back trajectories from the (a) Summit-2010 and (b) Tunu ice core sites over the period 2005-2013 C.E. Maps display the fraction of the total number of trajectory hours (~100000 hrs month^{-1}) spent within the total vertical column (under 10000 m). Back trajectories were allowed to travel for 10 days. New trajectories were started every 12 hours. Map grid resolution is 2°x2°. Ice core locations are shown by a pink circle. Maps show that air masses consistently arrive at Summit from the SE Greenland coast with a smaller contribution from the SW coast, consistent with the trajectories seen in the boundary layer (Fig. 5). Air masses consistently arrive at Tunu from the western Greenland coast with a smaller contribution from the SE.

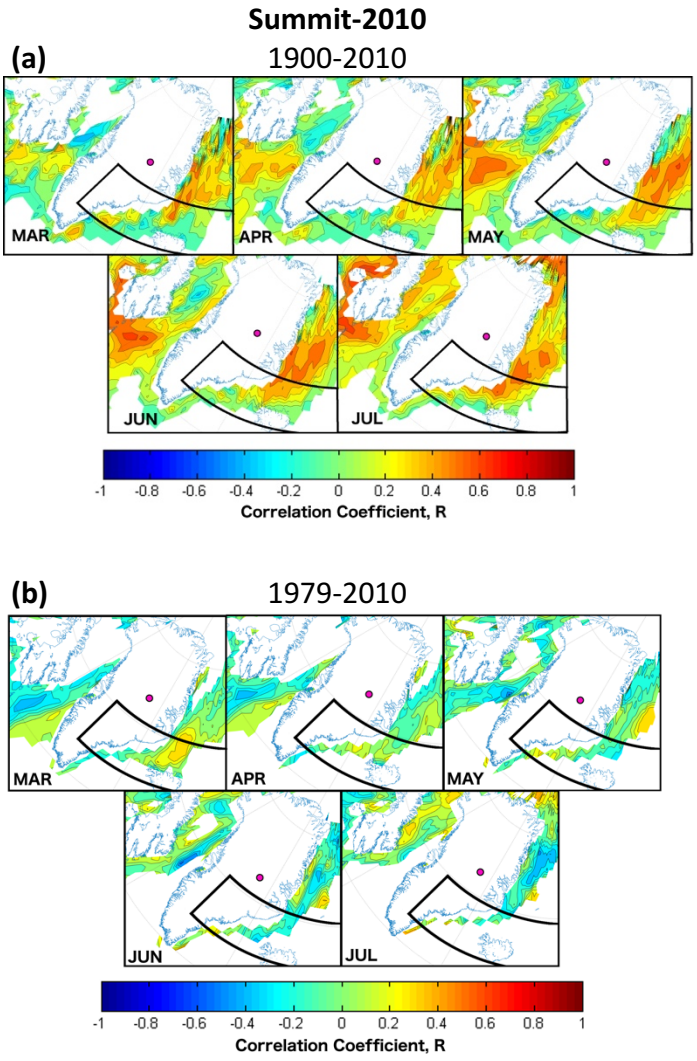

Figure S9. Correlation maps of monthly sea ice concentration (SIC) derived from the Summit-2010 ice core. (a) HadISST1 ICE dataset from 1900-2010 C.E. correlated with annual records of MSA. Outliers were removed from the MSA records before the correlations were performed to prevent distortion of the correlations. Month labels indicate the month of SIC compared with the annual MSA value. Only locations that showed a SIC variability greater than 10% and have a significant correlation (t-test, $p<0.05$) are displayed. The area of sea ice that is the likely source of MSA (as indicated by the air mass trajectories) are outlined in black [70°− 63°N, 0°− 45°W]. (b) As for (a) but focused on the satellite period 1979-2010 C.E..

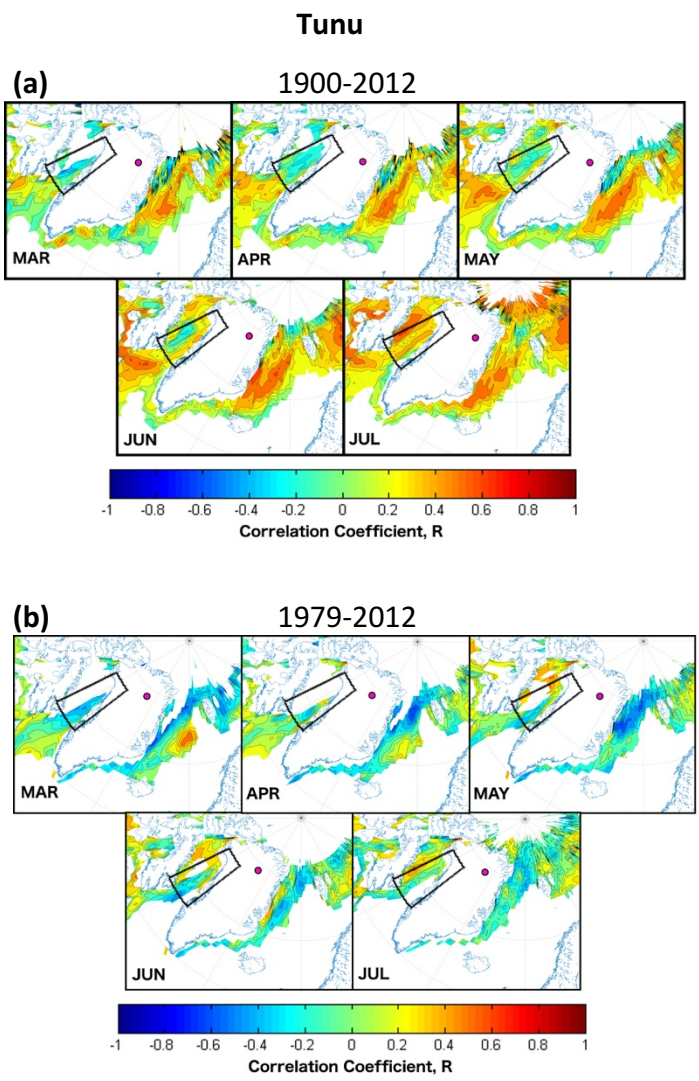

Figure S10. Correlation maps of monthly sea ice concentration (SIC) derived from the Tunu ice core. (a) HadISST1 ICE dataset from 1900-2012 C.E. correlated with annual records of MSA. Outliers were removed from the MSA records before the correlations were performed to prevent distortion of the correlations. Month labels indicate the month of SIC compared with the annual MSA value. Only locations that showed a SIC variability greater than 10% and have a significant correlation (t-test, $p<0.05$) are displayed. The area of sea ice that is the likely source of MSA (as indicated by the air mass trajectories) are outlined in black [77°−67°N, 62°−50°W]. (b) As for (a) but focused on the satellite period 1979-2012 C.E.

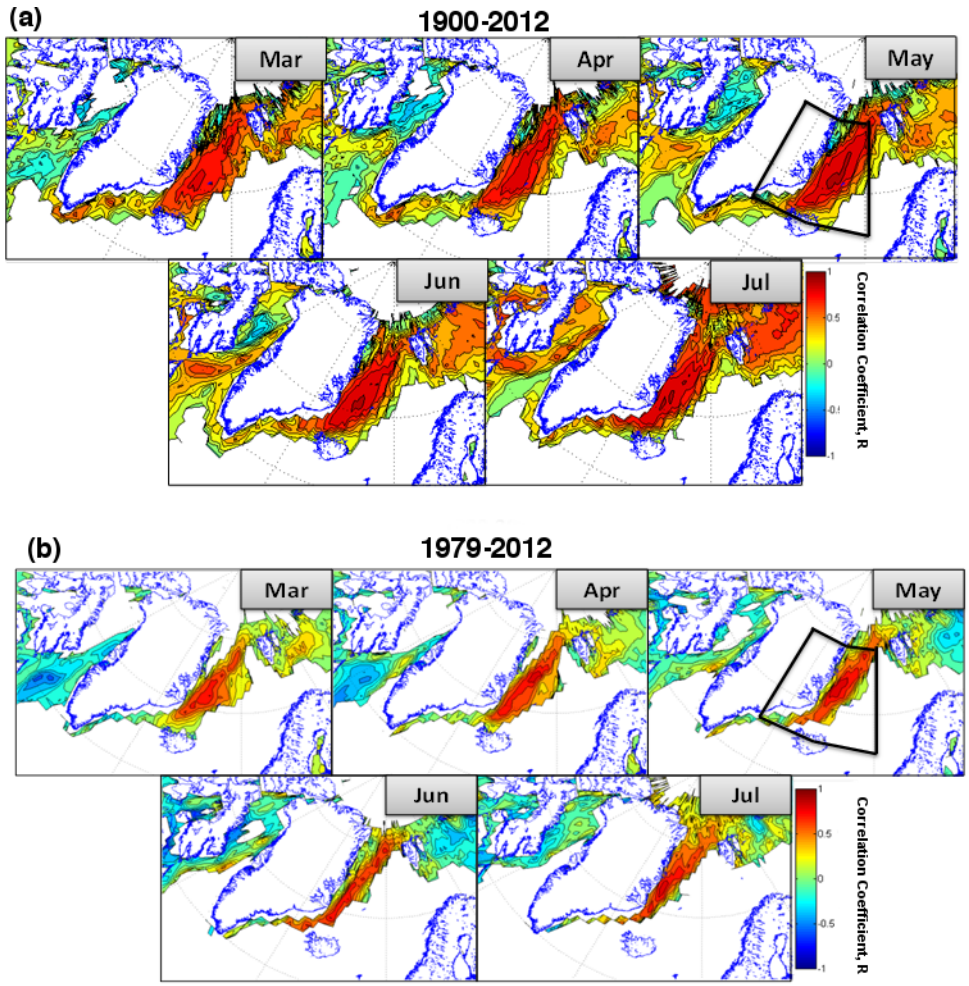

Figure S11. Autocorrelation maps of SIC during (a) the extended era (1900−2012 C.E.) and (b) satellite era (1979−2012 C.E.). Monthly SIC values were compared with the average SIC record from the area which shows the high positive correlation to the Summit-2010 MSA record (outlined in black in Figs. 6a, 6b). There is clearly a negative correlation between sea ice on the east and west coast which is seen over both era from March through to May, but the relationship turns positive in June and July over the extended time period (1900−2012 C.E.)

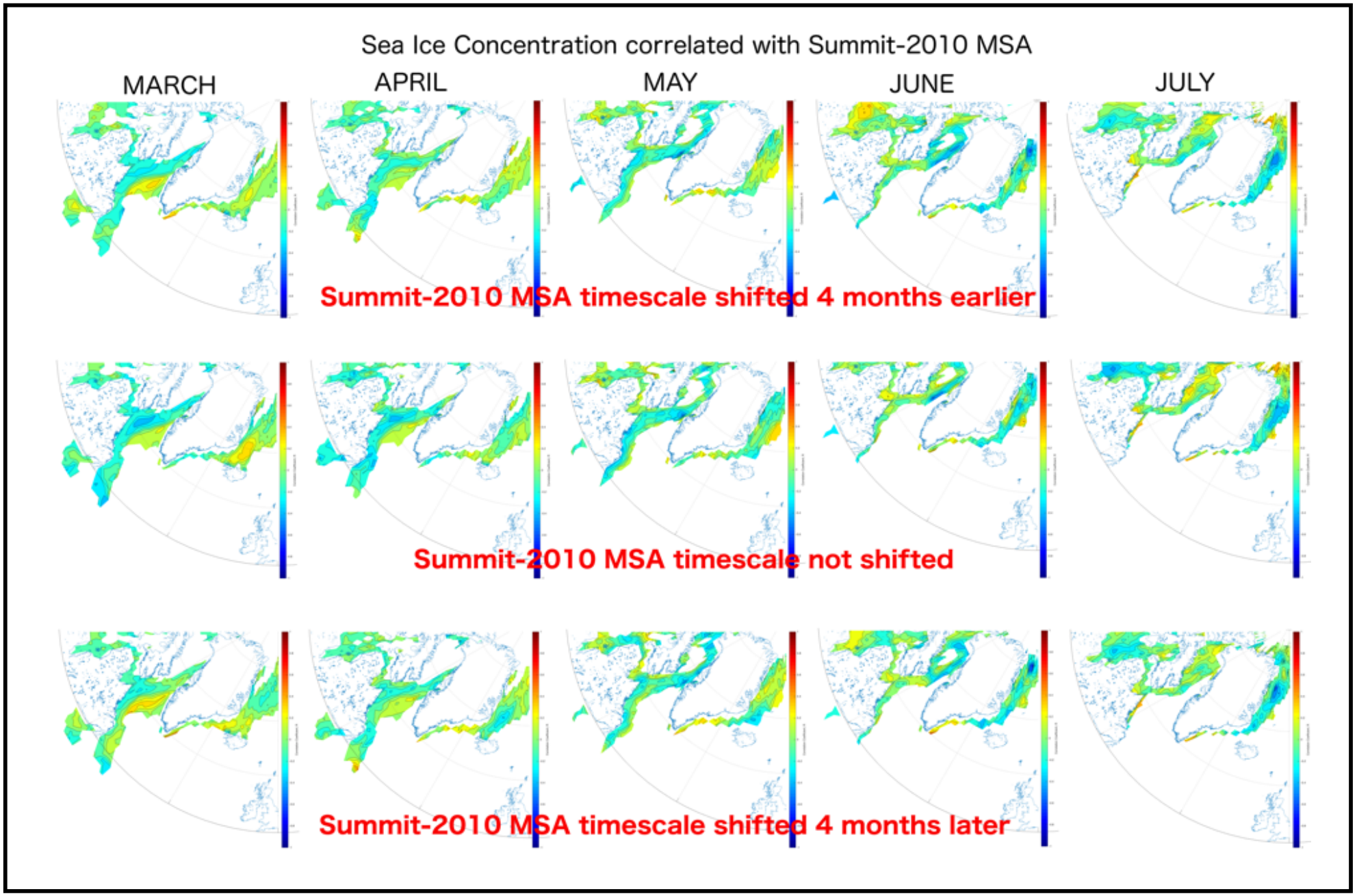
Sea Ice Concentration correlated with Summit-2010 MSA
MARCH
APRIL
MAY
JUNE
JULY
Summit-2010 MSA timescale shifted 4 months earlier
Summit-2010 MSA timescale not shifted
Summit-2010 MSA timescale shifted 4 months later

Figure S12

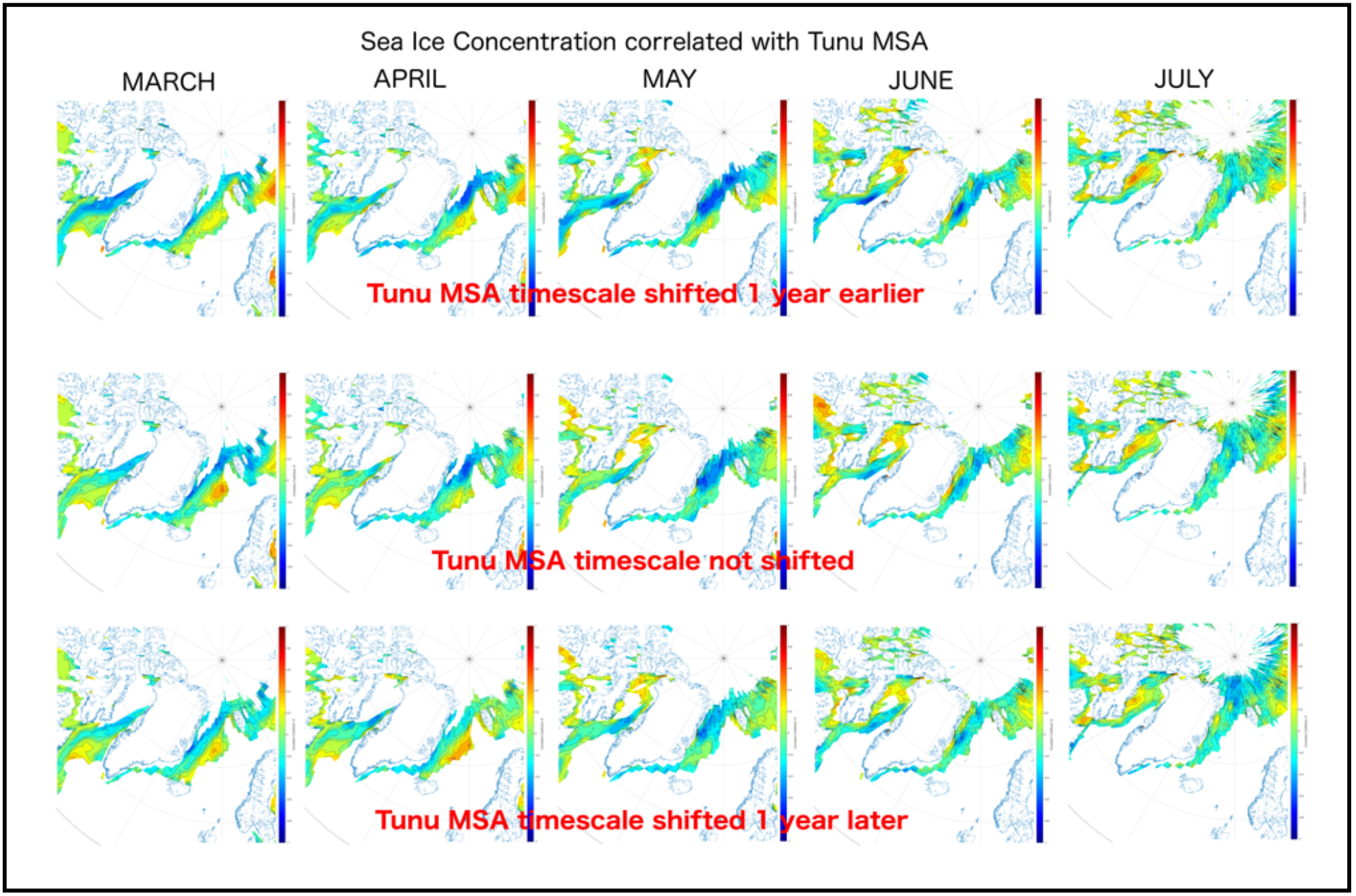

Figure S12 continued

Figure S12. Analysis of the effect of errors in the ice core timescales on the correlation between the site MSA record and the local sea ice concentrations (SIC). By shifting the dating of the MSA records to either extreme of the dating error estimate and replotting the SIC correlation plots (Figs. 6 and 7) it is clear the error in the dating of the MSA records does not affect the sign of the correlations displayed on the maps but can have an affect on the magnitude of the correlation found in different locations. This is likely a result of the peaks in the MSA record being shifted in or out of temporal coherence with peaks in SIC at the different locations.

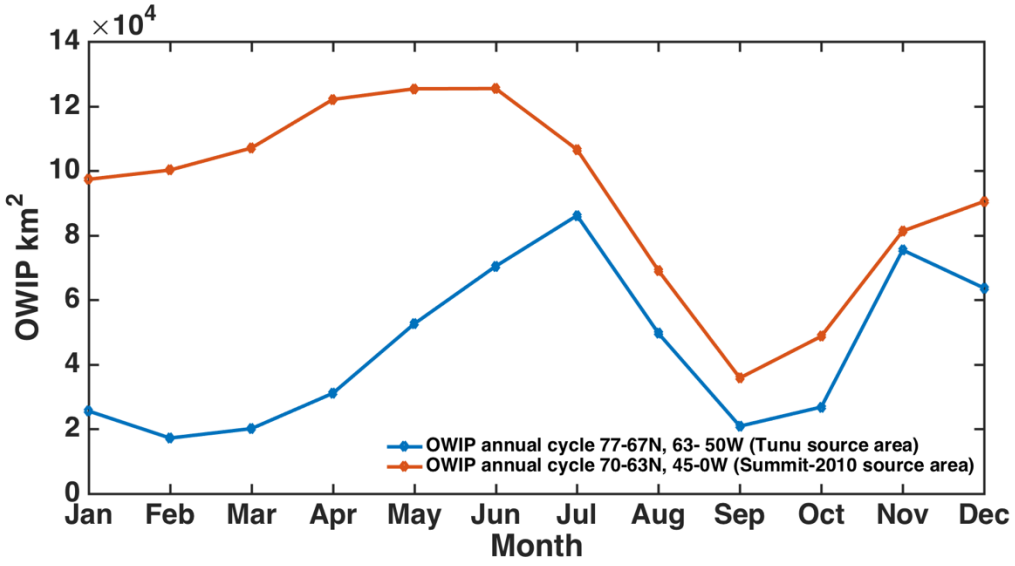

Figure S13: Annual cycle of open water in the ice pack (OWIP) within the aerosol source regions designated in Figs. 6 and 7. The annual cycle has been averaged over the period 1900-2012. The satellite period 1979-2012 shows the same temporal variability in OWIP at both sites but at reduced OWIP values.

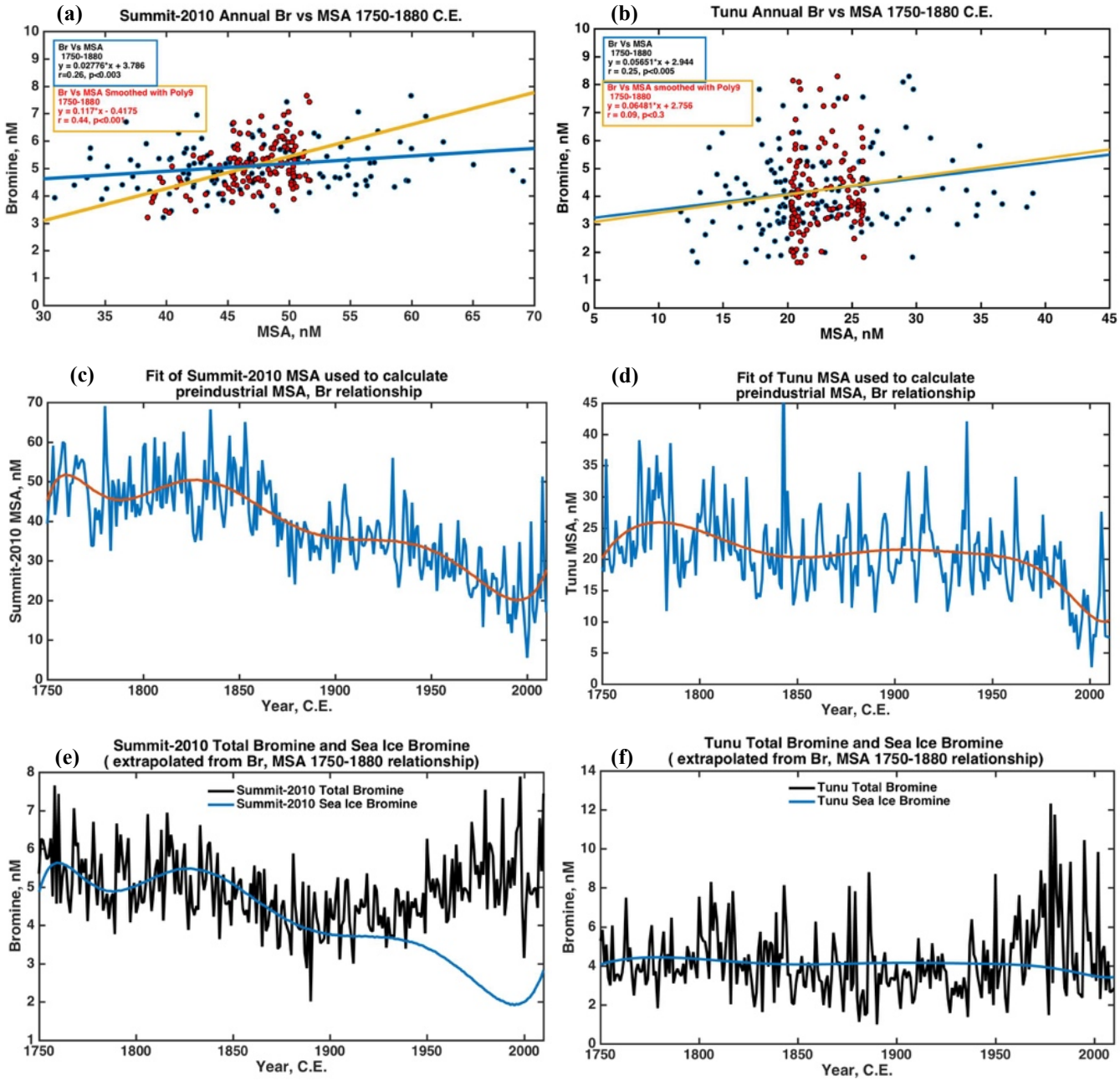

Figure S14: Summary of the technique used to determine nsiBr: the amount of Bromine in excess of what is expected from a purely sea ice source. (a,b) Blue dots, blue fit line: correlation plots between total bromine and total MSA in Summit-2010 and Tunu ice cores, respectively over the preindustrial period 1750-1880 C.E.. Red dots, yellow fit line: Correlation plots between total bromine and smoothed MSA time series shown in c and d. (c,d) Annual MSA record fit with 9th order polynomial. (e,f) Comparison between the total bromine record (black) and the bromine predicted from the smoothed MSA, Br linear relationship determined in a and b (blue) – the bromine from a purely sea ice source. The difference between the blue and black lines in panels

1 e and f is the amount of bromine in excess of what is expected from a purely sea ice source (nsiBr; see Fig.
2 8).

3

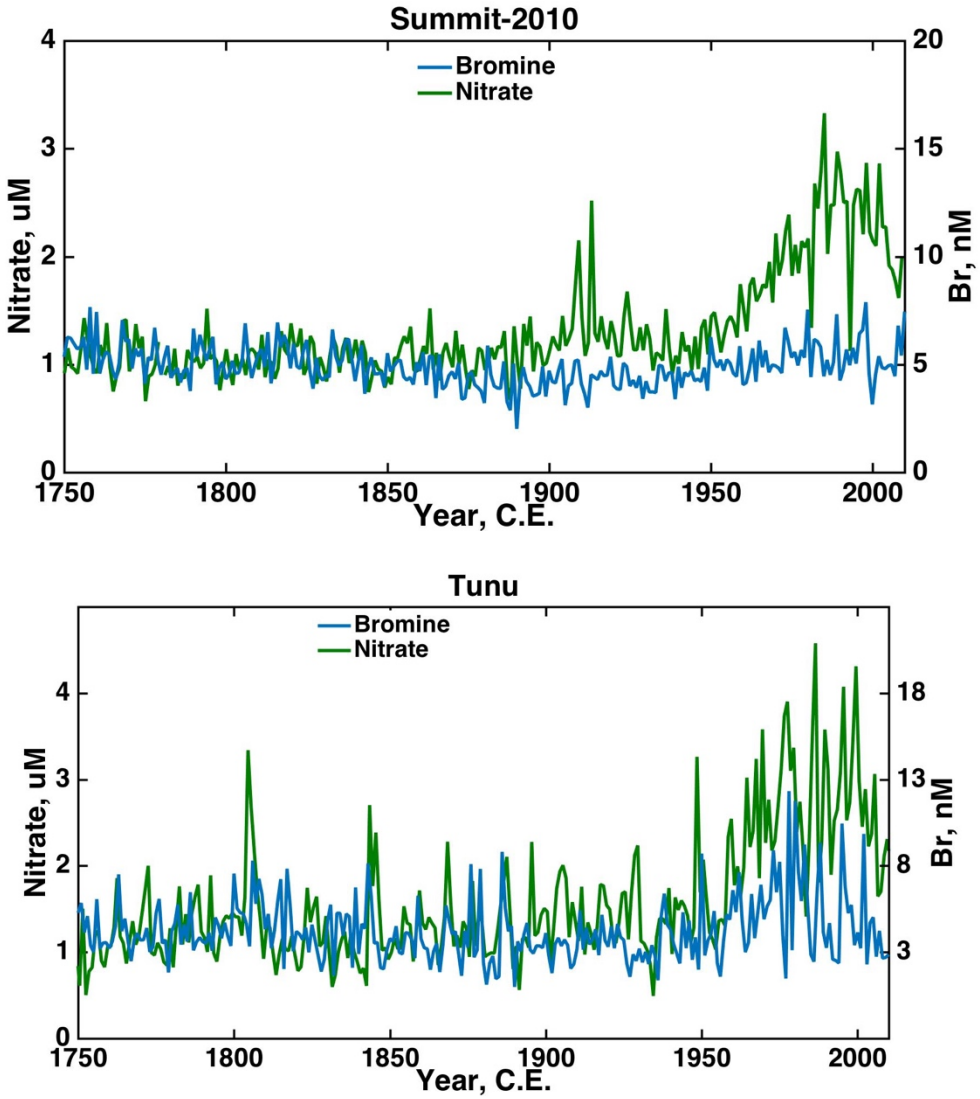

Figure S15: Comparison between nitrate and bromine records at both ice core sites. The difference between the two time-series is most dramatic at the Summit-2010 site because the sea ice record changes most dramatically at this site – and sea ice is the underlying driver of the bromine record.

References

Legrand, M., Hammer, C., De Angelis, M., Savarino, J., Delmas, R., Clausen, H. and Johnsen, S. J.: Sulfur-containing species (methanesulfonate and SO4) over the last climatic cycle in the Greenland Ice Core Project (central Greenland) ice core, J. Geophys. Res., 102(C12), 26663, doi:10.1029/97JC01436, 1997.

Mulvaney, R., Pasteur, E. C., Peel, D. A., Saltzman, E. S. and Whung, P.-Y.: The ratio of MSA to non-sea-salt sulphate in Antarctic Peninsula ice cores, Tellus B, 44(4), doi:10.3402/tellusb.v44i4.15457, 1992.

Weller, R.: Postdepositional losses of methane sulfonate, nitrate, and chloride at the European Project for Ice Coring in Antarctica deep-drilling site in Dronning Maud Land, Antarctica, J. Geophys. Res., 109(D7), 1–9, doi:10.1029/2003JD004189, 2004.